Volume 41 | Number 24 | 21 December 2017 | Pages 14775–15626

NJC

New Journal of Chemistry

A journal for new directions in chemistry

rsc.li/njc

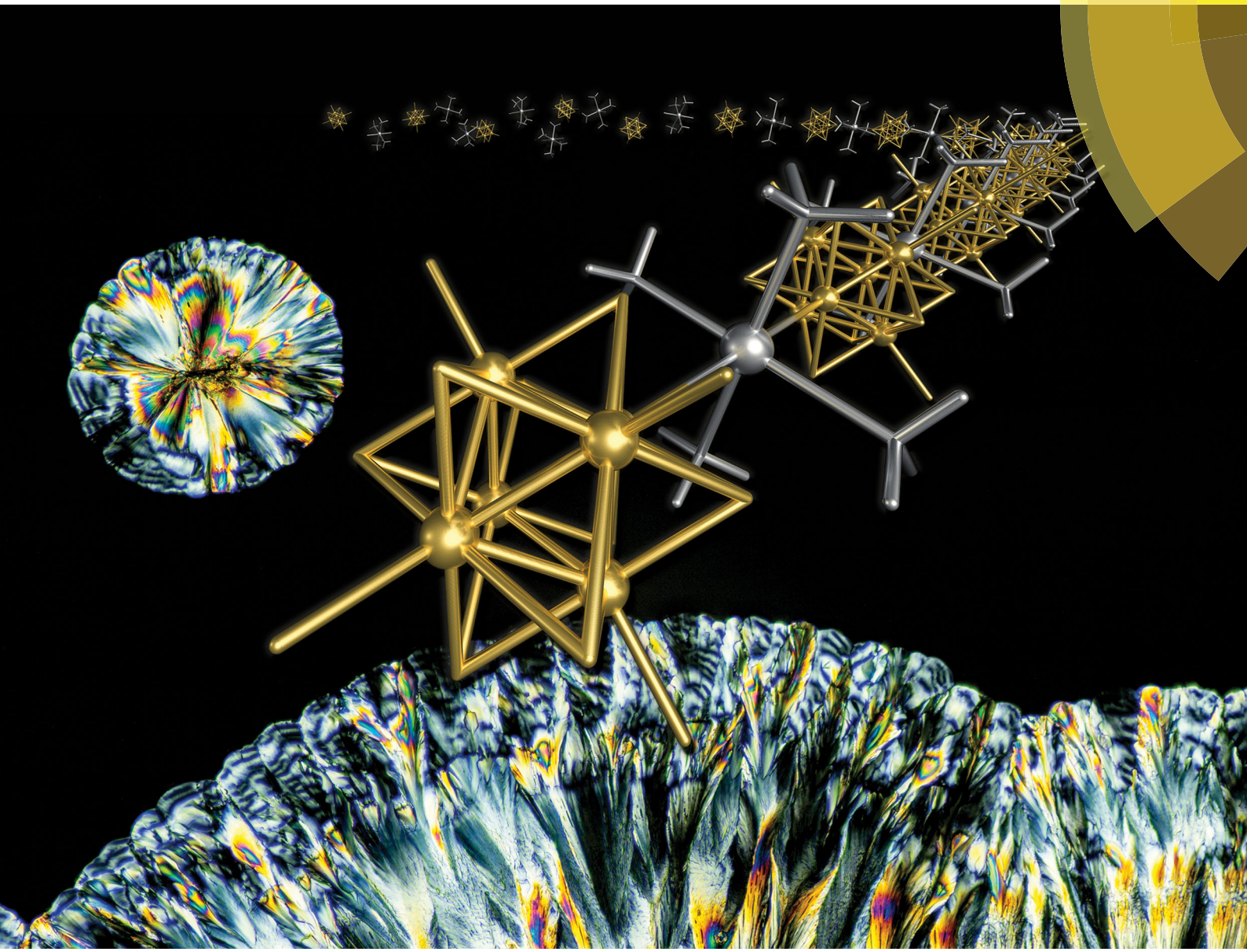

ISSN 1144-0546

ROYAL SOCIETY OF CHEMISTRY

PAPER

Olga A. Efremova, Michael A. Shestopalov *et al.*

Luminescent coordination polymers based on Ca^{2+} and octahedral cluster anions $[\{M_6Cl^i_8\}Cl^a_6]^{2-}$ (M = Mo, W): synthesis and thermal stability studies

cnrs

NJC

PAPER

View Article Online
View Journal | View Issue

Cite this: *New J. Chem.*, 2017, **41**, 14855

Luminescent coordination polymers based on Ca^{2+} and octahedral cluster anions $[\{M_6Cl^i_8\}Cl^a_6]^{2-}$ (M = Mo, W): synthesis and thermal stability studies†

Darya V. Evtushok,[ab] Natalya A. Vorotnikova,[ab] Vladimir A. Logvinenko,[ac] Anton I. Smolentsev,[ac] Konstantin A. Brylev,[abc] Pavel E. Plyusnin,[ac] Denis P. Pishchur,[a] Noboru Kitamura,[d] Yuri V. Mironov,[abc] Anastasiya O. Solovieva,[b] Olga A. Efremova*[e] and Michael A. Shestopalov*[abc]

Received 2nd August 2017,
Accepted 13th October 2017

DOI: 10.1039/c7nj02858j

rsc.li/njc

Luminescent coordination polymers (CPs) based on inexpensive stable precursors are attractive materials for applications. Here we report the synthesis and evaluation of the stability and photophysical characteristics of the first examples of phosphorescent CPs based on octahedral molybdenum and tungsten cluster anions. In particular, 1D CP *trans*-$[\{Ca(OPPh_3)_4\}\{\{M_6Cl^i_8\}Cl^a_6\}]_\infty$ (M = Mo, W) can be obtained either directly at increased temperature or *via* intermediate phases $[cis\text{-}Ca(OPPh_3)_4(H_2O)_2][\{M_6Cl^i_8\}Cl^a_6]\cdot 2CH_3CN$ that are stable at room-temperature, but convert to the titled CPs at temperatures above 100 °C.

Introduction

Coordination polymers (CPs) are a versatile class of compounds researched worldwide due to their potential in many areas including gas storage, sensing, photonics, electronics, drug delivery, *etc.* These compounds are typically assembled from simple building units – metal cations or cationic complexes and bridging ligands, where both the nature of the building units and the final structure determine the properties of the CPs. The predominant majority of the CPs currently developed employ organic polydentate ligands as linkers between the metal cationic centres, while those that employ inorganic linkers are relatively scarce, due to the limited number of such linkers. In the past two decades some members of our team and other groups have succeeded in employing a range of inorganic metal clusters as such linkers to develop metal-cluster based CPs that demonstrated properties such as homochirality,[1,2] high porosity,[3–5] ion conductivity,[6] luminescence[7] and magnetism.[8–10]

For the development of luminescent materials octahedral cluster anions of molybdenum and tungsten of the general formula $[\{M_6X^i_8\}L^a_6]^{2-}$ (where M is Mo or W; X is an inner halogen ligand; L is an apical inorganic or organic apical ligand) are extremely attractive building blocks. Indeed, depending on X and L, some members of this family demonstrate intensive luminescence in the red/near-infrared region with emission lifetimes of hundreds of microseconds and often with significant quantum yields.[11–17] Due to these properties, materials based on these clusters have been demonstrated to have potential in solar energy harvesting,[18,19] bioimaging, photodynamic therapy,[20–22] photo-catalysis,[23–27] oxygen sensing,[28–31] lighting,[32–34] *etc.*

In order to work as a linker with another metal centre, the apical ligands L of a metal cluster should be ambidentate. On the other hand, in order to develop a photoluminescent material based on a CP of a metal cluster, the cluster should not only be highly luminescent, but ideally also be stable in the presence of water and upon heating. Unfortunately, among the known molybdenum and tungsten anions there are only a handful of them that satisfy all of the above criteria and $[\{M_6X^i_8\}X^a_6]^{2-}$ (M is Mo or W; X is a halogen atom) are among them. Indeed these cluster anions are well-known for their luminescence properties[35] and they are stable over a wide temperature range and in aqueous solution.[29]

The choice of the cationic part and any of the supporting ligands for a CP should be driven by their coordination ability,

[a] *Nikolaev Institute of Inorganic Chemistry SB RAS, 3 Acad. Lavrentiev Prospect, 630090 Novosibirsk, Russia. E-mail: shtopy@niic.nsc.ru; Tel: +73833309253*
[b] *Research Institute of Clinical and Experimental Lymphology – Branch of the ICG SB RAS, 2 Timakova Str., 630060 Novosibirsk, Russia*
[c] *Novosibirsk State University, 2 Pirogova st., 630090 Novosibirsk, Russia*
[d] *Department of Chemistry, Faculty of Science, Hokkaido University, 060-0810 Sapporo, Japan*
[e] *School of Mathematics and Physical Sciences, University of Hull, Cottingham Road, HU6 7RX, Hull, UK. E-mail: o.efremova@hull.ac.uk; Tel: +44 (0)1482 465417*

† Electronic supplementary information (ESI) available: Tables with crystallographic data; and FTIR, XRPD, TGA, DTG, and DSC curves and related data. CCDC 1565898–1565900 (**1**, **2** and **4**). For ESI and crystallographic data in CIF or other electronic format see DOI: 10.1039/c7nj02858j

electronic state that would not quench the luminescence of the cluster, transparency in the visible region of the spectra, and cost. Therefore, here we present the synthesis, crystal structures, stability studies and luminescence properties of new cluster compounds based on the cationic complexes of calcium coordinated by triphenylphosphine oxide ($OPPh_3$) and cluster anions $[\{M_6Cl^i_8\}Cl^a_6]^{2-}$. Namely, ionic compounds $[cis\text{-}Ca(OPPh_3)_4(H_2O)_2][\{M_6Cl^i_8\}Cl^a_6]\cdot 2CH_3CN$, where M is Mo (**1**) or W (**2**), were obtained by direct crystallisation from water/acetonitrile solution. Upon heating, these compounds converted into 1D CPs $trans\text{-}[\{Ca(OPPh_3)_4\}\{\{M_6Cl^i_8\}Cl^a_6\}]_\infty$ (M = Mo (**3**), W (**4**)). Compounds **3** and **4** were also obtained directly by crystallisation at high temperature.

Experimental

Materials and methods

Cluster compound $(H_3O)_2[\{Mo_6Cl^i_8\}Cl^a_6]\cdot 6H_2O$ was prepared as described in ref. 36, while $(H_3O)_2[\{W_6Cl^i_8\}Cl^a_6]\cdot 7H_2O$ was obtained according to ref. 37. All other reagents and solvents were purchased and used without further purification. The CHNS elemental analyses were performed on a EuroVector EA3000 Elemental Analyser. Energy dispersive spectroscopy (EDS) was performed on a Hitachi TM3000 Tabletop SEM with Bruker QUANTAX 70 EDS equipment. Infrared spectra were measured on KBr pellets with a Scimitar FTS 2000 spectrometer. X-ray powder diffraction data were collected on a Philips PW 1700 diffractometer using CuK_α radiation (λ = 1.5406 Å) and a graphite monochromator. Optical diffuse reflectance spectra were measured at room temperature on a Shimadzu UV-Vis-NIR 3101 PC spectrophotometer (Shimadzu Corporation, Kyoto, Japan) equipped with an integrating sphere and reproduced in the form of Kubelka–Munk theory.

For emission measurements, powdered samples were placed between two non-fluorescent glass plates. The measurements were carried out at 298 K. The samples were excited by 355 nm laser pulses (6 ns duration, LOTIS TII, LS-2137/3). Corrected emission spectra were recorded on a red-light-sensitive multichannel photodetector (Hamamatsu Photonics, PMA-11). For emission decay measurements, the emission was analysed using a streakscope system (Hamamatsu Photonics, C4334 and C5094). The emission quantum yields were determined using an Absolute Photo-Luminescence Quantum Yield Measurement System (Hamamatsu Photonics, C9920-03), which comprised an excitation xenon light source (the excitation wavelength was set at 400 nm), an integrating sphere, and a red-sensitive multichannel photodetector (Hamamatsu Photonics, PMA-12).

Synthetic procedures

Synthesis of $[cis\text{-}Ca(OPPh_3)_4(H_2O)_2][\{M_6Cl^i_8\}Cl^a_6]\cdot 2CH_3CN$ (M = Mo (1), W (2)). $CaCl_2\cdot 6H_2O$ (93 mg, 0.42 mmol) and $OPPh_3$ (465 mg, 1.68 mmol) were dissolved in 20 mL of water/acetonitrile solution (1 : 4). After that $(H_3O)_2[\{M_6Cl^i_8\}Cl^a_6]\cdot nH_2O$ (0.14 mmol, M = Mo or W) was added to the reaction mixture and stirred for 5 min. The yellow solution was slowly cooled to room temperature and was left to stand overnight in air for crystallisation. Yellow crystals of $[cis\text{-}Ca(OPPh_3)_4(H_2O)_2][\{M_6Cl^i_8\}Cl^a_6]\cdot 2CH_3CN$ were collected by filtration. Single crystals for X-ray structural analysis were separated manually from the precipitate (see the ESI,† Table S1).

Compound 1. Yield: 290 mg (88%). Anal. calc. for $C_{76}H_{70}CaCl_{14}Mo_6N_2O_6P_4$: C, 38.9; H, 3.0; N, 1.2 (%). Found: C, 38.5; H, 3.0; N, 1.2 (%). EDS shows a Mo : Ca : Cl : P ratio of 6 : 1.1 : 13.6 : 3.9 for $C_{76}H_{70}CaCl_{14}Mo_6N_2O_6P_4$. IR (KBr, cm^{-1}): 539s, 693s, 719s, 995m, 1118s (ν_{PO}), 1167s, 1434s, 1652m, 2260w (ν_{CN}), 3053m, 3495m (ν_{H_2O}) (Fig. S1, ESI†).

Compound 2. Yield: 334 mg (83%). Anal. calc. for $C_{76}H_{70}CaCl_{14}N_2O_6P_4W_6$: C, 31.8; H, 2.5; N, 1.0 (%). Found: C, 31.9; H, 2.5; N, 0.8 (%). EDS shows a W : Ca : Cl : P ratio of 6 : 1.1 : 14.2 : 3.9 for $C_{76}H_{70}CaCl_{14}N_2O_6P_4W_6$. IR (KBr, cm^{-1}): 537s, 696s, 721s, 995m, 1114s (ν_{PO}), 1169s, 1434s, 1650m, 2263w (ν_{CN}), 3052m, 3501m (ν_{H_2O}) (Fig. S2, ESI†).

Synthesis of $trans\text{-}[\{Ca(OPPh_3)_4\}\{\{M_6Cl^i_8\}Cl^a_6\}]_\infty$ (M = Mo (3), W (4)). $[cis\text{-}Ca(OPPh_3)_4(H_2O)_2][\{M_6Cl^i_8\}Cl^a_6]\cdot 2CH_3CN$ (M = Mo or W) (100 mg) were heated at 110 °C for 10 min. After cooling down the powders of $trans\text{-}[\{Ca(OPPh_3)_4\}\{\{M_6Cl^i_8\}Cl^a_6\}]_\infty$ (M = Mo (**3**), W (**4**)) were obtained (Fig. S3, ESI†).

Compound 4. Compound **4** was also prepared by heating a mixture of $(H_3O)_2[\{W_6Cl^i_8\}Cl^a_6]\cdot 6H_2O$ (175 mg, 0.10 mmol), $CaCl_2\cdot 6H_2O$ (22 mg, 0.10 mmol) and $OPPh_3$ (167 mg, 0.6 mmol) in 25 mL of water/acetonitrile solution (1 : 4) for 30 min at 60 °C, which resulted in the formation of a yellow crystalline precipitate. Yield: 272 mg (99%). Single crystals for X-ray structural analysis were separated manually from the precipitate (Table S1, ESI†).

Compound 3. Anal. calc. for $C_{72}H_{60}CaCl_{14}Mo_6O_4P_4$: C, 38.9; H, 2.7 (%). Found: C, 38.9; H, 2.8 (%). EDS shows a Mo : Ca : Cl : P ratio of 6 : 0.9 : 14.0 : 4.1 for $C_{72}H_{60}CaCl_{14}Mo_6O_4P_4$. IR (KBr, cm^{-1}): 539s, 689s, 724s, 995m, 1122s (ν_{PO}), 1178s, 1438s, 3449m (ν_{H_2O}) (Fig. S1, ESI†).

Compound 4. Anal. calc. for $C_{72}H_{60}CaCl_{14}W_6O_4P_4$: C, 31.4; H, 2.2 (%). Found: C, 31.7; H, 2.3 (%). EDS shows a W : Ca : Cl : P ratio of 6 : 1.1 : 14.3 : 3.9 for $C_{72}H_{60}CaCl_{14}Mo_6O_4P_4$. IR (KBr, cm^{-1}): 544s, 688s, 724s, 995m, 1120s (ν_{PO}), 1175s, 1431s, 3439m (ν_{H_2O}) (Fig. S2, ESI†).

X-ray crystal structure analysis

Single-crystal X-ray diffraction data were collected at 150 K on a Bruker Nonius X8 Apex 4K CCD diffractometer with graphite monochromatised MoK_α radiation (λ = 0.71073 Å). All crystallographic information is summarised in Table S1 (ESI†). Absorption corrections were made semi-empirically using the SADABS program.[38] The structures were solved using direct methods and refined using the full-matrix least-squares method using the SHELXTL program package.[38] All non-hydrogen atoms were refined anisotropically. The H atoms of the phenyl groups of $OPPh_3$ ligands and the methyl groups of solvate acetonitrile molecules were positioned geometrically and refined by using a riding model. The H atoms of coordinated water molecules were located from difference Fourier maps and refined in an isotropic approximation with fixed U_{iso} = 0.05 $Å^2$. The main

crystallographic data and structure refinement results are presented in Table S1 (ESI†). The selected bond lengths are listed in Table S2 (ESI†). The atomic positional and thermal parameters, and full lists of bond lengths and angles were deposited at CCDC 1565898–1565900 for compounds **1**, **2** and **4**, respectively.

Thermal analysis

Differential scanning calorimetry (DSC) measurements were performed using a heat flow measurement method on a Netzsch DSC 204 F1 Phoenix calorimeter over the 20–150 °C temperature range, at a heating rate of 6 °C min^{-1}, in an Ar flow of 25 mL min^{-1}. Simultaneous TG-DSC/EGA-MS measurements were performed in an apparatus consisting of an STA 449 F1 Jupiter thermal analyser and a QMS 403D Aëolos quadrupole mass spectrometer (NETZSCH, Germany). The spectrometer was connected online to a thermal analyser (STA) instrument by a quartz capillary heated to 280 °C. The QMS was operated with an electron impact ioniser with an energy of 70 eV. The ion currents of the selected mass/charge (m/z) numbers were monitored in multiple ion detection (MID) mode with a collection time of 1 s for each channel. The measurements were made in a helium flow in the 30–500 °C temperature range at the heating rate of 10 °C min^{-1}, the gas flow rate of 30 mL min^{-1}, in open Al_2O_3 crucibles. Thermogravimetric analyses (TGA) and kinetic experiments were carried out on a TG 209 F1 Iris thermobalance (NETZSCH, Germany). The measurements were made in a helium flow in the 30–800 °C temperature range at the heating rates of 5, 10 and 20 °C min^{-1}, the gas flow rate of 60 mL min^{-1}, in open Al_2O_3 crucibles. The sample masses were in the 10–15 mg range.

Thermogravimetric curves obtained with different heating rates were processed with the use of the 'Model-free' module of Netzsch Thermokinetics 2 (Version 2004.05) software to calculate the activation energy without preliminary information about the kinetic topochemical equation. The Friedman method was used to calculate the activation energies for each experimental point of fractional conversion in the $0.005 < \alpha < 0.995$ range. The same set of experimental data was then used to search for the corresponding topochemical equation. The selection was made from 16 equations: chemical reaction at the interface, nucleation and diffusion. For the initial calculation, a differential method with linear regression was used to calculate kinetic parameters, which were then refined using the nonlinear regression method to allow the kinetic analysis of multistage thermal decomposition reactions. The F test was used to search for the best kinetic description and for the statistical control of the obtained equation.

Results and discussion

Syntheses and characterisation

The interaction of the cluster $(H_3O)_2[\{M_6Cl^i_8\}Cl^a_6]$ (M = Mo, W) with $CaCl_2$ and $OPPh_3$ in a water/acetonitrile solution at room temperature produces ionic compounds $[cis\text{-}Ca(OPPh_3)_4(H_2O)_2][\{M_6Cl^i_8\}Cl^a_6]\cdot 2CH_3CN$, where M = Mo (**1**) and W (**2**), in good yields.

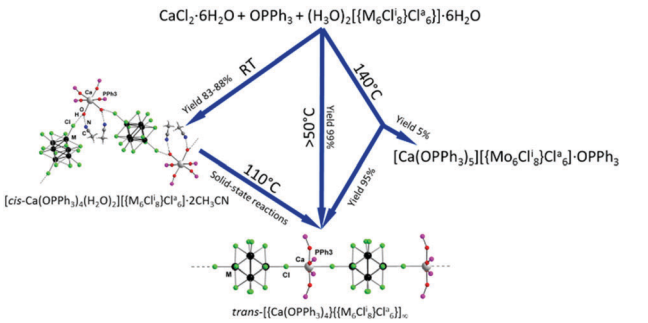

Scheme 1

When the same reactions were carried out at 50 °C or above the CP cluster compounds *trans*-$[\{Ca(OPPh_3)_4\}\{\{M_6Cl^i_8\}Cl^a_6\}]_\infty$ (M = Mo (**3**), W (**4**)) were formed. Upon heating at 110 °C for 10 min, **1** and **2** quantitatively converted into **3** and **4**, respectively. Notably, in an earlier study a similar reaction in excess of $OPPh_3$ under hydrothermal conditions led to $[Ca(OPPh_3)_5][\{Mo_6Cl^i_8\}Cl^a_6]\cdot OPPh_3$ as a by-product (Scheme 1).[39]

Compounds **1**, **2** and **4** were characterised using single-crystal X-ray diffraction analysis and the details of the experiment are summarised in Table S1, ESI.† Note that the crystal structure and the direct synthesis of compound **3** in boiling solvent were described earlier.[36]

Compounds **1** and **2** are isostructural and have ionic structures (monoclinic symmetry, space group: $C2/c$, $Z = 4$) composed of the discrete *cis*-$[Ca(OPPh_3)_4(H_2O)_2]^{2+}$ cationic units and molybdenum or tungsten cluster anions $[\{M_6Cl^i_8\}Cl^a_6]^{2-}$, respectively. The central calcium atom of the complex cation is located on the 2-fold axis $(0, y, \frac{1}{4})$, while the centre of the cluster coincides with the centrosymmetric special position (0, 0, 0). All other atoms are located in general positions. In complexes **1** and **2** Ca^{2+} has a typical distorted octahedral geometry[40] formed by the oxygen atoms of four $OPPh_3$ and two H_2O ligands in the *cis*-position to one another. $Ca–O_{OPPh_3}$ distances are in the 2.260(2)–2.337(2) Å range, while $Ca–O_{H_2O}$ bonds are equal to 2.409(2) Å for **1** and 2.378(8) Å for **2**. The cluster anion consists of a nearly perfect M_6 octahedron having eight μ_3-capping Cl^i and six apical Cl^a ligands. The bond lengths in the cluster anion are similar to those in the starting cluster complexes and related complexes (summarised in Table S2, ESI†).[36,37,39,41]

Apart from ionic bonding, the structures of **1** and **2** are supported by an extensive network of hydrogen bonds (Fig. 1). In particular, two solvate CH_3CN molecules are bound to each *cis*-$[Ca(OPPh_3)_4(H_2O)_2]^{2+}$ cation by hydrogen bonds N···H–O (2.77(2) Å for **1**, 2.83(3) Å for **2**). The cation also interacts with two cluster anions through hydrogen bonds O–H···Cl (3.33(5) Å for both **1** and **2**), which give rise to pseudo-polymeric zigzag chains running along the c axis. Moreover, each chain is connected to two adjacent chains by π–π stacking interactions between the phenyl rings of $OPPh_3$ ligands (average interplanar distances are about 3.8 Å). These interactions lead to the formation of infinite layers in the bc plane.

Compound **4** also belongs to the monoclinic symmetry with space group $C2/c$ and $Z = 4$, and is isostructural to

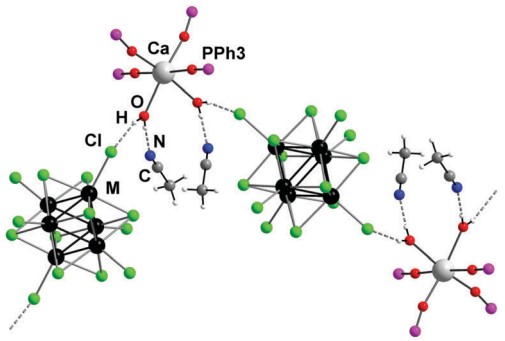

Fig. 1 Fragment of the structures of **1** and **2**, showing hydrogen bonding (dashed lines) between the [*cis*-Ca(OPPh$_3$)$_4$(H$_2$O)$_2$]$^{2+}$ cations, [{M$_6$Cl$^i_8$}-Cl$^a_6$]cluster anions and CH$_3$CN molecules. The Ph groups of the OPPh$_3$ are omitted for clarity.

compound **3**.[36] The structure of **4** is built up from linear polymeric chains directed along the *b* axis and has 2-fold axis symmetry. The chains are formed by nearly square-planar cationic units {Ca(OPPh$_3$)$_4$}$^{2+}$ connected to the {{W$_6$Cl$^i_8$}Cl$^a_6$}$^{2+}$ cluster anions *via* the apical *trans*-chlorine ligands (Fig. 2). The W–W, W–Cl^i and W–Cl^a distances (Table S2, ESI†) are comparable to those found in **2** and the related compounds.[37,41] At a supramolecular level, the chains are interconnected through π–π stacking interactions between the phenyl rings of OPPh$_3$ ligands with interplanar distances of about 3.7 Å.

Apart from the complexes described herein, there are only a few other Ca^{2+} complexes with triphenylphosphine oxide ligands in the Cambridge crystallographic database, including [Cp*Ca(OPPh$_3$)$_3$]I·CH$_3$C$_6$H$_5$,[42] [Ca(OPPh$_3$)$_2$(N(SiMe$_3$)$_2$)$_2$][43] and [Ca(OPPh$_3$)$_2$(CH(SiMe$_3$)$_2$)$_2$].[44] The Ca–O$_{OPPh_3}$ distances in **1**, **2** and **4** are close to the analogous distances in these complexes.

Transition of compounds **1** and **2** into **3** and **4** upon heating at 110 °C was confirmed by X-ray powder diffraction analysis. Indeed, the powder diffraction patterns of **3** and **4** generated by heating of **1** and **2** are in a good agreement with those calculated from the corresponding single-crystal data (Fig. S4 and S5, ESI†). Moreover, compounds **1–4** are stable under ambient conditions for a prolonged period of time (Fig. S6, ESI†). From the structural point of view, the phase transition involves the elimination of coordinated water molecules and the solvate acetonitrile, and the formation of new covalent bonds Cl^a–Ca–Cl^a combined with the *cis*- to *trans*-isomerisation in the coordination environment of Ca^{2+}. These processes lead to an overall reduction of the unit cell volumes of **1** and **2** by about 10%.

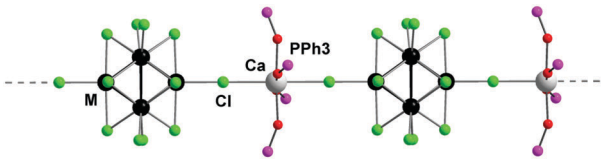

Fig. 2 The structure of *trans*-[{Ca(OPPh$_3$)$_4$}{{M$_6$Cl$^i_8$}Cl$^a_6$}]$_\infty$. Ph groups are omitted for clarity.

Thermal properties and kinetic analysis

To establish the transformation of **1** and **2** into CPs **3** and **4**, respectively, compounds **1** and **2** were characterised using TG-DTA at heating rates of 5, 10 and 20 K min^{-1}. According to TG measurements (Fig. 3 and Fig. S7, S8, ESI†) there is a one-step weight loss of 4.6% for **1** and 3.8% for **2** in the 70–120 °C temperature range. The values of the weight losses are close to those calculated for the elimination of two coordinated water molecules and two acetonitrile solvate molecules from compounds **1** (5.0%) and **2** (4.1%). The subsequent heating of the cluster complex (>340 °C) led to OPPh$_3$ ligand destruction followed by the decomposition of the cluster complexes.

Both DTA and mass spectrometry modalities of the method showed that there is only a very small (if any) temperature gap between the elimination of water and acetonitrile molecules (Fig. S9 and S10, ESI†). Calculation of the activation energies using the Friedman method of calculations applicable for a one-step process has not resulted in a constant value of the activation energies for each conversion point (Fig. S11 and S12, ESI†). The kinetic analysis of both molybdenum and tungsten systems was therefore carried out assuming the two-stage process (Fig. S13 and S14, ESI†): (**I**) A → B and (**II**) B → C. For molybdenum compound **1** the best fit of the modelled thermograms with the experiment was achieved when the first stage of the reaction was modelled by the Avrami–Erofeev equation, while the second one with the n^{th} order equation:

$$\mathbf{I}: f(\alpha)_1 = (1-\alpha)[-\ln(1-\alpha)]^{0.62}$$

$$\mathbf{II}: f(\alpha)_2 = (1-\alpha)^{0.58}$$

With this model the composition of intermediate B corresponded to the removal of 2.2 wt% of the solvent. The final refinement of the kinetic parameters gave the following values of the activation energy (E) and the pre-exponential factors (A):

$$\mathbf{I}: E_1 = 167 \pm 2 \text{ kJ mol}^{-1}, \lg A_1 = 23.1 \pm 0.3.$$

$$\mathbf{II}: E_2 = 44 \pm 3 \text{ kJ mol}^{-1}, \lg A_2 = 4.8 \pm 0.1.$$

The decomposition process of the tungsten compound **2** was successfully modelled as two consecutive processes that follow

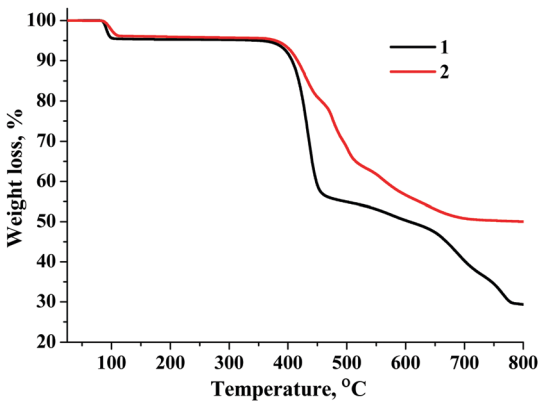

Fig. 3 TGA curves of **1** and **2**. Heating rates of 10 °C min^{-1}.

the Avrami–Erofeev equation, which corresponded to the removal of 22.3 wt% for intermediate B and gave the following kinetic parameters:

$$\mathbf{I}: f_1(\alpha) = (1-\alpha)[-\ln(1-\alpha)]^{0.17},\ E_1 = 212 \pm 10\ \text{kJ mol}^{-1},$$
$$\lg A_1 = 28.5 \pm 0.1.$$

$$\mathbf{II}: f_2(\alpha) = (1-\alpha)[-\ln(1-\alpha)]^{0.41},\ E_2 = 197 \pm 10\ \text{kJ mol}^{-1},$$
$$\lg A_2 = 27.8 \pm 0.2.$$

Notably, the phenomenon of staging was also observed in the DSC curves (Fig. S15 and S16, ESI†). Moreover, the staging was more pronounced for the molybdenum compound than for the tungsten one, which is in agreement with the calculated values of the activation energies for stages **I** and **II** for both compounds. Both reactions are endothermic, with total thermal effects calculated to be 205 and 206 kJ mol^{-1} for **1** and **2** respectively (Schemes S1 and S2, ESI†). There are several processes that should contribute to the thermal effect, which include the loss of energy to break covalent bonding Ca–O_{H_2O}, and hydrogen bonding Cl^a–O_{H_2O} and N–O_{H_2O}, and the energy gained from the formation of new Ca–Cl^a bonds in the $\{trans\text{-}Ca(OPPh_3)_4Cl^a{}_{2/2}\}$ unit. These bond energies do not depend on the composition of the cluster core and hence the enthalpy of the reaction also does not depend on the cluster.

In summary, the activation energies for the decomposition of the tungsten compound are higher than those of the molybdenum compound, while the enthalpies of the reactions are nearly the same. The possible explanation could be that the $\{W_6Cl^i_8\}^{4+}$ (M_w = 1383) cluster core is heavier and larger than $\{Mo_6Cl^i_8\}^{4+}$ (M_w = 867) that presumably would lead to increase in the activation energies associated with the transport of gas through the solid and rearrangement of the solid.

Optical properties

To analyse the optical properties of compounds **1–4**, we studied both absorption and luminescence properties. The diffuse reflectance spectra of **1–4** and the corresponding parent cluster compounds presented in the form of Kubelka–Munk theory are given in Fig. S17 and S18 (ESI†). Our data show that the replacement of the Bu_4N^+ by $\{Ca(OPPh_3)_4\}^{2+}$ has little effect on both the profile of the adsorption and the band-gap in the tungsten compounds, while in the case of molybdenum compounds **1** and **3** some shortening of the optical band gap by about 0.2 eV was observed.

Room temperature luminescence spectroscopic studies were performed for solid-state powder samples of **1–4** and for related compounds $(Bu_4N)_2[\{W_6Cl^i_8\}Cl^a_6]$. Luminescence characteristics emission maximum wavelengths (λ_{em}), emission quantum yields (Φ_{em}) and lifetimes (τ_{em}) of the compounds are summarised in Table 1, together with those previously reported for the solid samples of $(Bu_4N)_2[\{M_6Cl^i_8\}Cl^a_6]$. Upon 355 nm excitation, the compounds show emission similar to other metal cluster compounds based on the $\{M_6X_8\}^{4+}$ (M = Mo or W, X = Cl or Br) cluster core (Fig. 4). λ_{em} observed within the current study for $(Bu_4N)_2[\{M_6Cl^i_8\}Cl^a_6]$ (M = Mo or W) and τ_{em} determined for $(Bu_4N)_2[\{Mo_6Cl^i_8\}Cl^a_6]$ are comparable to those reported earlier[35] and thus can be used for validation of our results. It is worth noting that, to the best of our knowledge, Φ_{em} for $(Bu_4N)_2[\{M_6Cl^i_8\}Cl^a_6]$ (M = Mo or W) and τ_{em} for $(Bu_4N)_2[\{W_6Cl^i_8\}Cl^a_6]$ in the solid state have never been reported before. The emission maxima of the calcium-based compounds are slightly red-shifted for the hexamolybdenum complexes and blue-shifted for the tungsten compounds. Also, opposite tendencies are observed for changes in τ_{em} and Φ_{em} values: for **1** and **3** they are considerably higher, while for **2** and **4** they are appreciably lower than those for $(Bu_4N)_2[\{Mo_6Cl^i_8\}Cl^a_6]$ and $(Bu_4N)_2[\{W_6Cl^i_8\}Cl^a_6]$, respectively. However, there is a similarity

Table 1 Spectroscopic and photophysical properties of [*cis*-$Ca(OPPh_3)_4(H_2O)_2][\{M_6Cl^i_8\}Cl^a_6]\cdot 2CH_3CN$ (M = Mo (**1**), W (**2**)), *trans*-$[\{Ca(OPPh_3)_4\}\{\{M_6Cl^i_8\}Cl^a_6\}]_\infty$ (M = Mo (**3**), W (**4**)) and $(Bu_4N)_2[\{M_6Cl^i_8\}Cl^a_6]$ (M = Mo or W) in the solid state

Compound	λ_{em}, nm	τ_{em}, μs (*A*)	Φ_{em}
$(Bu_4N)_2[\{Mo_6Cl^i_8\}Cl^a_6]$	750 (760[a], 805[b])	127 (120[a])	0.15
1	750	133	0.20
3	740	215	0.31
$(Bu_4N)_2[\{W_6Cl^i_8\}Cl^a_6]$	800 (825[b])	7.8	0.12
2	790	3.4	0.06
4	780	4.9	0.07

[a] Ref. 45. [b] Ref. 35.

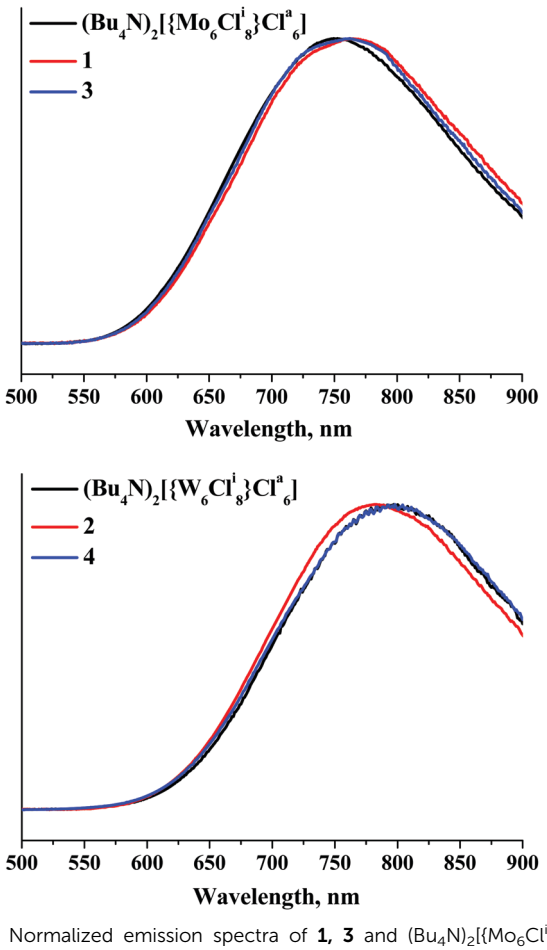

Fig. 4 Normalized emission spectra of **1**, **3** and $(Bu_4N)_2[\{Mo_6Cl^i_8\}Cl^a_6]$ (top) and **2**, **4** and $(Bu_4N)_2[\{W_6Cl^i_8\}Cl^a_6]$ (bottom) in the solid state.

in the changes in the luminescence properties of the studied compounds: τ_{em} and Φ_{em} determined for CPs *trans*-$[\{Ca(OPPh_3)_4\}\{\{M_6Cl^i_8\}Cl^a_6\}]_\infty$ are higher than those of the corresponding parent ionic compounds $[cis\text{-}Ca(OPPh_3)_4(H_2O)_2]$-$[\{M_6Cl^i_8\}Cl^a_6]\cdot 2CH_3CN$ for both M = Mo and M = W (Table 1). The lower values of luminescence quantum yields and lifetimes for aqua-complexes **1** and **2** in comparison with the corresponding CPs are likely due to energy dissipation through vibrations of H_2O.

The effect of the cationic part on the luminescence properties of octahedral anionic clusters have been discussed in several earlier works, where reasons such as energy transfer from the excited metal cluster to the cationic unit, in particular to the aromatic part of the cationic unit and self-absorption by the material, were discussed.[46–50] In the present system, however, we believe that the molecular packing structures in the solid state have effects on the luminescence. Indeed, it has recently been reported that the emission lifetime of $[\{Mo_6Cl^i_8\}Cl^a_6]^{2-}$ is very sensitive to the packing structures in the crystalline phase through the intermolecular interactions between the inner-Cl and apical-Cl ligands of the nearest neighbour cluster anion. Since the emissive excited state of $[\{Mo_6Cl^i_8\}Cl^a_6]^{2-}$ is localised primarily on the $\{Mo_6Cl^i_8\}^{4+}$-core, the perturbation to the cluster core influences strongly the emission properties.[51] The careful evaluation of the distances between the centers of cluster anions shows that in the case of the Ca compounds the shortest distances between neighbouring cluster anions (12.466 Å for **1** and 13.051 Å for **3**) are significantly longer than that for the Bu_4N^+ compounds (8.645 Å). This "isolation" of cluster anions would explain the longer τ_{em} and larger Φ_{em} for **1** and **3** in comparison with the corresponding Bu_4N^+ salt. We expected similar situations to those in the molybdenum crystalline phases to also emerge in the tungsten clusters. However, the tendency is opposite, *i.e.* although cluster anions are located further from each other, the emission quantum yields and the lifetimes of **2** and **4** are smaller and shorter, respectively. The opposite trend might be due to the more dense molecular packings of the tungsten compounds. Indeed, although the tungsten cluster anion is bigger than the molybdenum one, both the volumes of unit cells in **2** and **4** are smaller and Ca–Cl^a contacts are shorter than those in **1** and **3**. These intermolecular interactions can facilitate efficient non-radiative decay to the ground state or excitation energy migration between cluster anions and subsequent energy trapping by crystal defects.

Conclusions

In summary, we demonstrate the preparation of one-dimensional photoluminescent CPs based on cationic units $\{Ca(OPPh_3)_4\}^{2+}$ and photoluminescent cluster anions $[\{M_6Cl^i_8\}Cl^a_6]^{2-}$ (M = Mo or W). In particular, we demonstrate that CPs *trans*-$[\{Ca(OPPh_3)_4\}$-$\{\{M_6Cl^i_8\}Cl^a_6\}]_\infty$ are formed at increased temperature in a water/acetonitrile mixture and remain stable at room temperature and up to 340 °C. However, if the reaction is carried out at room temperature, ionic compounds $[cis\text{-}Ca(OPPh_3)_4(H_2O)_2]$-$[\{M_6Cl^i_8\}Cl^a_6]\cdot 2CH_3CN$ are formed. The latter can be viewed as an intermediate phase, since these compounds convert into more thermodynamically stable CP phases at increased temperature. Indeed, although the phase transition according to DSC studies has a large positive enthalpy contribution of around 205–206 kJ mol^{-1}, the conversation has a significant increase of the total entropy of the system that would not depend on the cluster composition. The kinetic parameters of the phase transition do, however, depend on the cluster core: the tungsten system is significantly more kinetically inert than the molybdenum one, as it is expressed by noticeably higher values of activation energy.

All four of the compounds studied demonstrate luminescence in the visible region. Notably, the photoluminescence lifetimes and quantum yields of the $[\{Mo_6Cl^i_8\}Cl^a_6]^{2-}$-based CPs almost doubled in comparison with those of $(Bu_4N)_2[\{Mo_6Cl^i_8\}Cl^a_6]$, while for the hexatungsten compounds the opposite tendency was observed.

Conflicts of interest

There are no conflicts of interest to declare.

Acknowledgements

This work was supported by RFBR according to research projects No. 17-03-00140 and No. 16-34-00542.

Notes and references

1 Y. V. Mironov, N. G. Naumov, K. A. Brylev, O. A. Efremova, V. E. Fedorov and K. Hegetschweiler, *Angew. Chem., Int. Ed.*, 2004, **43**, 1297–1300.
2 Y. V. Mironov, N. G. Naumov, K. A. Brylev, O. A. Efremova, V. E. Fedorov and K. Hegetschweiler, *Russ. J. Coord. Chem.*, 2005, **31**, 269–281.
3 N. G. Naumov, A. V. Virovets and V. E. Fedorov, *Inorg. Chem. Commun.*, 2000, **3**, 71–72.
4 M. A. Shestopalov, A. Y. Ledneva, S. Cordier, O. Hernandez, M. Potel, T. Roisnel, N. G. Naumov and C. Perrin, *Angew. Chem., Int. Ed.*, 2011, **50**, 7300–7303.
5 N. Ding, G. S. Armatas and M. G. Kanatzidis, *J. Am. Chem. Soc.*, 2010, **132**, 6728–6734.
6 O. A. Efremova, E. O. Golenko, Y. V. Mironov, N. K. Moroz, C.-C. Wang and V. E. Fedorov, *J. Phys. Chem. C*, 2007, **111**, 11008–11011.
7 Y. V. Mironov, V. E. Fedorov, H. Bang and S.-J. Kim, *Eur. J. Inorg. Chem.*, 2006, 553–557.
8 S. Kim, Y. Kim, J. Lee, W. Shin, M. Lee and S.-J. Kim, *Inorg. Chim. Acta*, 2007, **360**, 1890–1894.
9 Y. M. Litvinova, Y. M. Gayfulin, D. G. Samsonenko, A. S. Bogomyakov, W. H. Shon, S.-J. Kim, J.-S. Rhyee and Y. V. Mironov, *Polyhedron*, 2016, **115**, 174–179.
10 Y. M. Litvinova, Y. M. Gayfulin, A. S. Bogomyakov, D. G. Samsonenko and Y. V. Mironov, *J. Cluster Sci.*, 2017, DOI: 10.1007/s10876-10017-11276-z.

11 M. N. Sokolov, M. A. Mihailov, E. V. Peresypkina, K. A. Brylev, N. Kitamura and V. P. Fedin, *Dalton Trans.*, 2011, **40**, 6375–6377.
12 K. Kirakci, P. Kubát, M. Dušek, K. Fejfarová, V. Šícha, J. Mosinger and K. Lang, *Eur. J. Inorg. Chem.*, 2012, 3107–3111.
13 O. A. Efremova, M. A. Shestopalov, N. A. Chirtsova, A. I. Smolentsev, Y. V. Mironov, N. Kitamura, K. A. Brylev and A. J. Sutherland, *Dalton Trans.*, 2014, **43**, 6021–6025.
14 M. A. Mikhailov, K. A. Brylev, P. A. Abramov, E. Sakuda, S. Akagi, A. Ito, N. Kitamura and M. N. Sokolov, *Inorg. Chem.*, 2016, **55**, 8437–8445.
15 O. A. Efremova, Y. A. Vorotnikov, K. A. Brylev, N. A. Vorotnikova, I. N. Novozhilov, N. V. Kuratieva, M. V. Edeleva, D. M. Benoit, N. Kitamura, Y. V. Mironov, M. A. Shestopalov and A. J. Sutherland, *Dalton Trans.*, 2016, **45**, 15427–15435.
16 D. V. Evtushok, A. R. Melnikov, N. A. Vorotnikova, Y. A. Vorotnikov, A. A. Ryadun, N. V. Kuratieva, K. V. Kozyr, N. R. Obedinskaya, E. I. Kretov, I. N. Novozhilov, Y. V. Mironov, D. V. Stass, O. A. Efremova and M. A. Shestopalov, *Dalton Trans.*, 2017, **46**, 11738–11747.
17 S. Akagi, S. Fujii, T. Horiguchi and N. Kitamura, *J. Cluster Sci.*, 2017, **28**, 757–772.
18 Y. Zhao and R. R. Lunt, *Adv. Energy Mater.*, 2013, **3**, 1143–1148.
19 A. Renaud, F. Grasset, B. Dierre, T. Uchikoshi, N. Ohashi, T. Takei, A. Planchat, L. Cario, S. Jobic, F. Odobel and S. Cordier, *ChemistrySelect*, 2016, **1**, 2284–2289.
20 A. O. Solovieva, Y. A. Vorotnikov, K. E. Trifonova, O. A. Efremova, A. A. Krasilnikova, K. A. Brylev, E. V. Vorontsova, P. A. Avrorov, L. V. Shestopalova, A. F. Poveshchenko, Y. V. Mironov and M. A. Shestopalov, *J. Mater. Chem. B*, 2016, **4**, 4839–4846.
21 A. Beltrán, M. Mikhailov, M. N. Sokolov, V. Pérez-Laguna, A. Rezusta, M. J. Revillo and F. Galindo, *J. Mater. Chem. B*, 2016, **4**, 5975–5979.
22 C. Felip-León, C. A. del Valle, V. Pérez-Laguna, M. I. Millán-Lou, J. F. Miravet, M. Mikhailov, M. N. Sokolov, A. Rezusta-López and F. Galindo, *J. Mater. Chem. B*, 2017, **5**, 6058–6064.
23 A. Barras, S. Cordier and R. Boukherroub, *Appl. Catal., B*, 2012, **123-124**, 1–8.
24 P. Kumar, S. Kumar, S. Cordier, S. Paofai, R. Boukherroub and S. L. Jain, *RSC Adv.*, 2014, **4**, 10420–10423.
25 P. Kumar, H. P. Mungse, S. Cordier, R. Boukherroub, O. P. Khatri and S. L. Jain, *Carbon*, 2015, **94**, 91–100.
26 S. Kumar, O. P. Khatri, S. Cordier, R. Boukherroub and S. L. Jain, *Chem. – Eur. J.*, 2015, **21**, 3488–3494.
27 M. Feliz, M. Puche, P. Atienzar, P. Concepción, S. Cordier and Y. Molard, *ChemSusChem*, 2016, **9**, 1963–1971.
28 R. N. Ghosh, G. L. Baker, C. Ruud and D. G. Nocera, *Appl. Phys. Lett.*, 1999, **75**, 2885–2887.
29 D. J. Osborn III, G. L. Baker and R. N. Ghosh, *J. Sol-Gel Sci. Technol.*, 2005, **36**, 5–10.
30 L. Riehl, M. Ströbele, D. Enseling, T. Jüstel and H.-J. Meyer, *Z. Anorg. Allg. Chem.*, 2016, **642**, 403–408.
31 R. N. Ghosh, P. A. Askeland, S. Kramer and R. Loloee, *Appl. Phys. Lett.*, 2011, **98**, 221103.
32 Y. Molard, *Acc. Chem. Res.*, 2016, **49**, 1514–1523.
33 T. G. Truong, B. Dierre, F. Grasset, N. Saito, N. Saito, T. K. N. Nguyen, K. Takahashi, T. Uchikoshi, M. Amela-Cortes, Y. Molard, S. Cordier and N. Ohashi, *Sci. Technol. Adv. Mater.*, 2016, **17**, 443–453.
34 O. A. Efremova, K. A. Brylev, Y. A. Vorotnikov, L. Vejsadová, M. A. Shestopalov, G. F. Chimonides, P. Mikes, P. D. Topham, S.-J. Kim, N. Kitamura and A. J. Sutherland, *J. Mater. Chem. C*, 2016, **4**, 497–503.
35 A. W. Maverick, J. S. Najdzionek, D. MacKenzie, D. G. Nocera and H. B. Gray, *J. Am. Chem. Soc.*, 1983, **105**, 1878–1882.
36 Z. S. Kozhomuratova, Y. V. Mironov, M. A. Shestopalov, Y. M. Gaifulin, N. V. Kurat'eva, E. M. Uskov and V. E. Fedorov, *Russ. J. Coord. Chem.*, 2007, **33**, 1–6.
37 P. A. Abramov, A. V. Rogachev, M. A. Mikhailov, A. V. Virovets, E. V. Peresypkina, M. N. Sokolov and V. P. Fedin, *Russ. J. Coord. Chem.*, 2014, **40**, 259–267.
38 *Bruker, APEX2 (Version 1.08), SAINT (Version 07.03), SADABS (Version 02.11), SHELXTL (Version 06.12)*, Bruker AXS Inc., Madison, WI, USA, 2004.
39 M. A. Shestopalov, A. I. Smolentsev, Z. S. Kozhomuratova, V. E. Fedorov and Y. V. Mironov, *Russ. J. Coord. Chem.*, 2012, **38**, 50–54.
40 A. K. Katz, J. P. Glusker, S. A. Beebe and C. W. Bock, *J. Am. Chem. Soc.*, 1996, **118**, 5752–5763.
41 D. H. Johnston, C. M. Brown, A. S. Yu and J. C. Gallucci, *Acta Crystallogr.*, 2010, **C66**, m303–m306.
42 K. C. Jayaratne, L. S. Fitts, T. P. Hanusa and V. G. Young, *Organometallics*, 2001, **20**, 3638–3640.
43 A. G. M. Barrett, M. R. Crimmin, M. S. Hill, G. Kociok-Köhn, D. J. MacDougall, M. F. Mahon and P. A. Procopiou, *Organometallics*, 2008, **27**, 3939–3946.
44 M. S. Hill, M. F. Mahon and T. P. Robinson, *Chem. Commun.*, 2010, **46**, 2498–2500.
45 A. W. Maverick and H. B. Gray, *J. Am. Chem. Soc.*, 1981, **103**, 1298–1300.
46 Y. A. Vorotnikov, M. Mikhailov, K. A. Brylev, D. A. Piryazev, N. V. Kuratieva, M. N. Sokolov, Y. V. Mironov and M. A. Shestopalov, *Russ. Chem. Bull.*, 2015, **64**, 2591–2596.
47 B. Dierre, K. Costuas, N. Dumait, S. Paofai, M. Amela-Cortes, Y. Molard, F. Grasset, Y. Cho, K. Takahashi, N. Ohashi, T. Uchikoshi and S. Cordier, *Sci. Technol. Adv. Mater.*, 2017, **18**, 458–466.
48 Y. A. Vorotnikov, O. A. Efremova, N. A. Vorotnikova, K. A. Brylev, M. V. Edeleva, A. R. Tsygankova, A. I. Smolentsev, N. Kitamura, Y. V. Mironov and M. A. Shestopalov, *RSC Adv.*, 2016, **6**, 43367–43375.
49 K. Kirakci, P. Kubát, M. Kučeráková, V. Šícha, H. Gbelcová, P. Lovecká, P. Grznárová, T. Ruml and K. Lang, *Inorg. Chim. Acta*, 2016, **441**, 42–49.
50 M. S. Tarasenko, A. Y. Ledneva, N. V. Kurat'eva, D. Y. Naumov, S.-J. Kim, V. E. Fedorov and N. G. Naumov, *Russ. J. Coord. Chem.*, 2007, **33**, 876–885.
51 N. Kitamura, Y. Kuwahara, Y. Ueda, Y. Ito, S. Ishizaka, Y. Sasaki, K. Tsuge and S. Akagi, *Bull. Chem. Soc. Jpn.*, 2017, **50**, 1164–1173.